Titanium Containing γ-MnO_2 (TM) Hollow Spheres: One-Step Synthesis and Catalytic Activities in Li/Air Batteries and Oxidative Chemical Reactions

By *Lei Jin, Linping Xu, Christine Morein, Chun-hu Chen, Monique Lai, Saminda Dharmarathna, Arthur Dobley,* and *Steven L. Suib**

Titanium containing γ-MnO_2 octahedral molecular sieves having hollow sphere structures are successfully prepared for the first time using a one-step synthesis method. Titanium cations are used as structure-directing agents in the synthesis process. The assembly of the hollow spheres is carried out at the beginning of the process. Various techniques including XRD, N_2 adsorption, SEM, EDX, RAMAN, TEM, XPS, and TGA are employed for the materials characterization. Ti is incorporated into the MnO_2 framework in isolated sites, and TiO_2 phases (anatase and rutile) are not observed. When introduced in medium-sized lithium-air batteries, the materials give very high specific capacity (up to 2.3 A h g^{-1}). These materials are also catalytically tested in the oxidation of toluene with molecular oxygen at atmospheric pressure, showing significant oxidative catalytic activities in this difficult chemical reaction.

1. Introduction

The preparation of nanomaterials of defined structures and composition, with tailored properties, has attracted immense scientific and technological interest due to the fact that morphologies and structures play a very important role in determining the catalytic, magnetic, and electric properties of materials.[1,2] Control of structures of nanomaterials has been one of the most challenging issues faced by materials scientists. Many efforts have been focused on self-assembly of nano-particles into two –dimensional (2D) and three-dimensional (3D) well-ordered hollow spheres, nanorods/nanowires and several hierarchical structures. For example, hierarchical ZnO nanostructures, penniform $BaWO_4$ nanostructures, a trigonal Se nanowire network, and dandelion-like CuO nanostructures have been successfully prepared.[3–6] However, it is still a significant challenge to develop low temperature, facile, solution-based, shape-controlled, and template free self-assembly routes for the formation of hierarchical structures.

Nanostructured hollow spheres and their related structures have either possess, or are proposed to have, diverse and fascinating applications, such as catalysts,[7] drug delivery,[8] high efficiency photodecomposition,[9] and low density batteries or devices.[10] Their syntheses often rely on complicated templating approaches, in which hard (e.g., inorganic, metal, and polymer particles) or soft sacrificial templates (e.g., supramolecular assemblies of surfactant and polymer) were used to create a hollow structure.[11–14] However, template contamination mostly decreases the activity of synthesized materials and the removal of residues is difficult.

Titanium containing materials have attracted attention in catalysis, solar cells, gas sensors, and semiconductors in recent decades.[15–19] For example, there is a great interest in titanium containing zeolite catalysts for selective oxidation recently. The titanium silicalites with MFI (TS-1) or MEL (TS-2) zeolite structures are remarkable redox catalysts in numerous friendly environmental applications.[20] Titanium-containing zeolites have become some of the most commercially significant catalysts for green peroxide oxidation of organic molecules.[21] However, titanium-containing γ-MnO_2 octahedral molecular sieves (TM) with significantly enhanced catalytic activity has rarely been reported.

Manganese oxide structures can form mixed-valent octahedral molecular sieves (OMS). These OMS materials have applications in energy storage, acid catalysts, and ion-exchange processes.[22–27] An electrochemically and catalytically active manganese oxide OMS is γ-MnO_2. This form of MnO_2 octahedral molecular sieve (also called chemical manganese dioxide, CMD), a disordered 1 × 1 and 1 × 2 tunnel structure corner shared with MnO_6 octahedral chains,[28] is one of these most useful manganese oxides and has been widely applied in the battery industry because of its high activity, low cost of raw materials, and low toxicity. Conventionally, γ-MnO_2 was synthesized by electrolysis (EMD), redox reactions,

[*] L. Jin, Dr. L. Xu, C.-h. Chen, M. Lai, S. Dharmarathna, Prof. S. L. Suib
Department of Chemistry
University of Connecticut
Institute of Materials Science
University of Connecticut
U-3060, 55 North Eagleville Rd., Storrs, Connecticut 06269 (USA)
E-mail: Steven.Suib@uconn.edu
C. Morein, Dr. A. Dobley
Yardney Technical Products Inc.
82 Mechanic Street, Pawcatuck, Connecticut 06379 (USA)

DOI: 10.1002/adfm.201001080

or disproportionation. However, to the best of our knowledge, the γ-MnO_2 prepared using the above methods having irregular morphologies, low surface area (<80 m^2 g^{-1}), and easy one-step synthesis of γ-MnO_2 hollow spheres with high surface area (>87 m^2 g^{-1}) has never been reported.

Li/air batteries have recently attracted interest due to the largest theoretical specific energy (11 972 W h kg^{-1}) among all practical electrochemical couples.[29–32] In a Li/air battery, the cathode material, oxygen is absorbed directly from the environment during the discharge process. The electrochemical reactions involved are described below:

$$4Li(s) + O_2(g) \rightarrow 2Li_2O(s)V = 2.91V \quad (1)$$

$$2Li(s) + O_2(g) \rightarrow Li_2O_2(s)V = 3.10V \quad (2)$$

The air cathodes are composed of a mixture of carbon powder, O_2 reduction catalysts, and a binder, and the nature of the catalyst plays a key role in delivering high specific capacities.[29] γ-MnO_2 based materials have been widely used in traditional batteries. However, the use of γ-MnO_2 materials as efficient O_2 reduction catalysts in the Li/air battery is novel.

Development of efficient heterogeneous catalysts for a solvent free toluene oxidation system has also received considerable attention due to their convenient use and facile recycling.[33–37] For example, Wang et al. reported liquid phase toluene oxidation with molecular oxygen over copper-based metal oxides. In this process, however, in order to observe good conversion, a closed capacity autoclave, oxygen pressure, and higher temperature (T > 160 °C) were used. These common reaction conditions are too dangerous due to the explosion hazards of toluene-oxygen vapors at high reaction temperatures.[28,38] From our previous work, we investigated the solvent free atmospheric oxidation of toluene in the presence of molecular oxygen using synthesized γ-MnO_2 OMS as the efficient heterogeneous catalyst.[28] More efficient oxidation catalysts are still needed.

In this work, a simple one-step precipitation synthesis of titanium containing γ-MnO_2 OMS hollow spheres with enhanced catalytic activity is first reported without adding surfactants or templates. Herein, Ti ion was used as the morphology directing agent in the precipitation process. With the addition of titanium ions, the obtained γ-MnO_2 octahedral molecular sieves have hollow spherical morphologies and high surface areas (>87 m^2 g^{-1}).

A high charge storage capacity (2.2 A h g^{-1} carbon) was obtained in the lithium air battery tests by using the reported titanium containing γ-MnO_2 hollow spheres as the O_2 reduction catalyst. In addition, synthesized γ-MnO_2 OMS have promising catalytic activities in the atmospheric oxidation of toluene in the presence of molecular oxygen.[28] In this work, the obtained γ-MnO_2 has significantly enhanced catalytic activity in this difficult liquid phase toluene oxidation process.

2. Results

2.1. X-ray Diffraction (XRD)

The phase purity of the products was investigated by conventional XRD experiments, as shown in **Figure 1**. All of the peaks

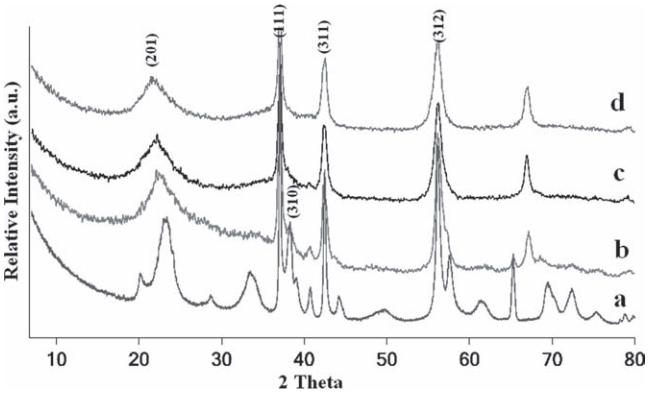

Figure 1. A representative XRD pattern recorded for γ–MnO_2 synthesized in this work. a) pure γ–MnO_2; b) 2 at% Ti/Mn; c) 4 at% Ti/Mn; d) 8 at% Ti/Mn.

match the reference data of a pure γ-MnO_2 phase.[39] The broadening of the (201) peak is known to occur for certain types of random intergrowths of ramsdellite (1 × 2) tunnel structure and pyrolusite (1 × 2 tunnel structure) of manganese dioxide based on the "De Wolff model" published in 1959.[40] Materials with different loadings of titanium ions were also investigated by XRD. Without Ti loading, a pure γ-MnO_2 phase (1 × 1 and 1 × 2 intergrowth tunnel structure manganese oxide) was obtained. After Ti-loading, as shown by Figure 1b for a typical sample with Ti/Mn = 2:100 atomic ratio (TM-3), all the peaks can be assigned to the γ-MnO_2 structure, but with broader peaks. The greater amount Ti loading led to broader patterns. These patterns are evidence of smaller particle size and higher surface area than found for the non-Ti loaded γ-MnO_2 materials. After 8 at% Ti loading, the γ-MnO_2 structure was maintained (Figure 1d) with no other phases, including Ti or TiO_2 phases present. However, under similar synthesis conditions, an anatase TiO_2 sample was obtained when no $MnSO_4$ and $KMnO_4$ were used.

2.2. Surface Area (SA), Porosity, and Energy Dispersive X-ray Spectroscopy (EDX)

N_2 physisorption for selected titanium containing γ-MnO_2 material (TM-1, Ti/Mn = 8:100, 8 at%) shows a typical isotherm with hysteresis for that of porous materials, shown in **Figure 2**. The insert in Figure 2 shows a broad mesopore distribution calculated by the BJH method. The 8% Ti containing γ-MnO_2 has pores with average diameters of 37 Å. The BET surface area of the material is higher than those of materials without Ti incorporation, as summarized in **Table 1**. EDXS data reveal the existence of manganese and titanium. No potassium was obtained. Fixed ratios of Ti/Mn around 0.02, 0.04, and 0.08 were observed as designed. The EDXS results are also summarized in Table 1.

2.3. Scanning Electron Microscope (SEM) and Transmission Electron Microscopy (TEM)

Figure 3 shows typical morphologies of pure γ-MnO_2 and the selected Ti-containing γ-MnO_2 (TM-1). A nano-fiber like

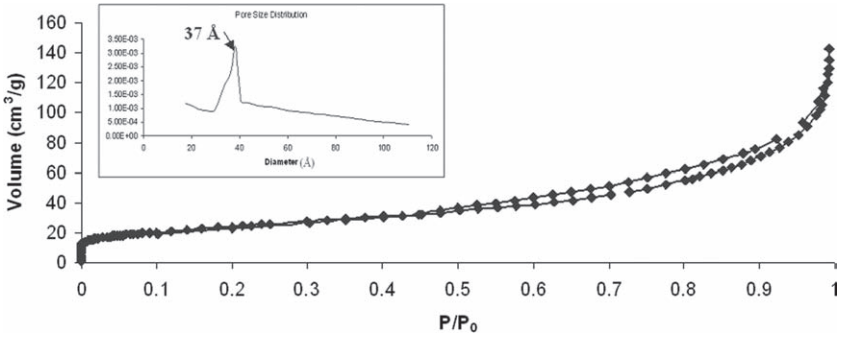

Figure 2. Pore size distribution of selected Ti containing γ-MnO_2 (TM-1).

morphology for pure γ-MnO_2 (Figure 3a) with an average diameter of about 50 nm was observed. However, after Ti incorporation, the morphology changed to hollow nanospheres composed of nano-flakes with an average flake thickness of about 15 nm. Both SEM and TEM images show a uniform morphology for the Ti-containing γ-MnO_2 and the pure γ-MnO_2.

The hollow nature of the synthesized material (TM-1) was confirmed by TEM imaging (Figure 3e and 3f). The diameters of the hollow shells range from 200 to 500 nm. The high magnification image reveals a shell thickness of 50 nm (Figure 3f). Increasing the magnification in Figure 3f clearly reveals the lattice fringes of a flake showing the lattice spacing of the (110) planes, $d \sim 3.2$ Å. No extra phases were observed for the hollow spheres even down to the 5 nm scale. The features observed in the TEM images also show broken lattice fringes, which correspond to structural defects and distortion of γ-MnO_2 as reported in the literature.[40–43] These defects and distortions are important for the catalytic activity of the γ-MnO_2.[41]

2.4. Thermogravimetric Analysis (TGA)

The thermal stability of the synthesized materials was analyzed by TGA measurements in N_2 atmosphere. As illustrated in **Figure 4**, all of the materials only show major weight losses for temperatures higher than 450 °C. The weight loss is related to release of oxygen in the structure causing a structural collapse similar to other OMS materials. With increasing of Ti incorporating levels from 0% to 8%, temperatures for structural collapse decrease from around 520 °C (pure γ-MnO_2) to 450 °C (TM-3, 2 at% Ti), 460 °C (TM-2, 4 at% Ti), and 470 °C (TM-1, 8 at% Ti). In addition, compared to the pure γ-MnO_2, after Ti incorporation, the materials did not show any extra weight loss peaks.

2.5. Raman Spectroscopy

Raman spectroscopy was used to study the presence of Ti in the framework of the γ-MnO_2 octahedral molecular sieves. Various authors have used Raman techniques to study transition metal atoms in the framework of molecular sieves.[44–47] Raman spectra of titanium containing γ-MnO_2 are shown in **Figure 5**. The peaks of MnO_2 located around 600–650 cm^{-1} are overlapped with a strong band of TiO_2 in this region. Raman patterns of pure anatase TiO_2 clearly showed peaks at 394.2, 513.4 and 637.6 cm^{-1}. Physically mixed 8 mol% TiO_2 with γ-MnO_2 (pure γ-MnO_2 synthesized using the procedure mentioned above) also showed peaks at 394.2 cm^{-1} and 513.4 cm^{-1}, indicating an anatase tetragonal structure assigned to the $2B_{1g}$ mode (394.2 cm^{-1} and 513.4 cm^{-1}) for the space group $D_{4h/19}$. However, the synthesized Ti containing manganese oxides showed no peaks in this area. With increasing contents (higher Ti/Mn molar ratio) in the samples, the peaks of MnO_2 located around 600 – 650 cm^{-1} were shifted and broaden. No additional peaks were present for any TiO_2 crystalline phase or Ti=O bond vibrations (from TiO^{2+} species).

2.6. X-ray Photoelectron Spectroscopy (XPS)

XPS was used to analyze the binding energy (BE) values and the atomic surface concentration of the corresponding elements present in the as-obtained Ti containing γ-MnO_2 molecular sieve (8 at% Ti/Mn). The XPS survey spectrum reveals that the 8% Ti containing γ-MnO_2 sample consists of the elements Ti, Mn, and O, no other impurities such as potassium ions or elemental sulfur are detected. The Mn 2p core level spectrum (**Figure 6a** inset) illustrates that the observed values of the binding energies for Mn 2p 3/2 and Mn 2p 1/2 (641.6 and 653.1 eV, respectively) are in good agreement with the literature values for MnO_2. The Ti 2p core level spectrum (Figure 6a inset) showed binding energies of 458.8 eV and 464.3 eV for Ti 2p 3/2 and Ti 2p 1/2 respectively. To define the difference in BE values from Ti-O-Ti binding present in TiO_2 and Ti-O-Mn in the γ-MnO_2 framework is difficult. The

Table 1. BET surface area of synthesized materials and EDXS results on titanium analysis.

Sample ID	BET surface area [m^2 g^{-1}]	EDXS analysis		
		Detecting Elements	Theoretical [at %]	Experimental [at %]
Pure γ-MnO_2	18	Ti	0	0
2% Ti/Mn	59	Ti	2	1.9
4% Ti/Mn	77	Ti	4	3.5
8% Ti/Mn	87	Ti	8	7.5

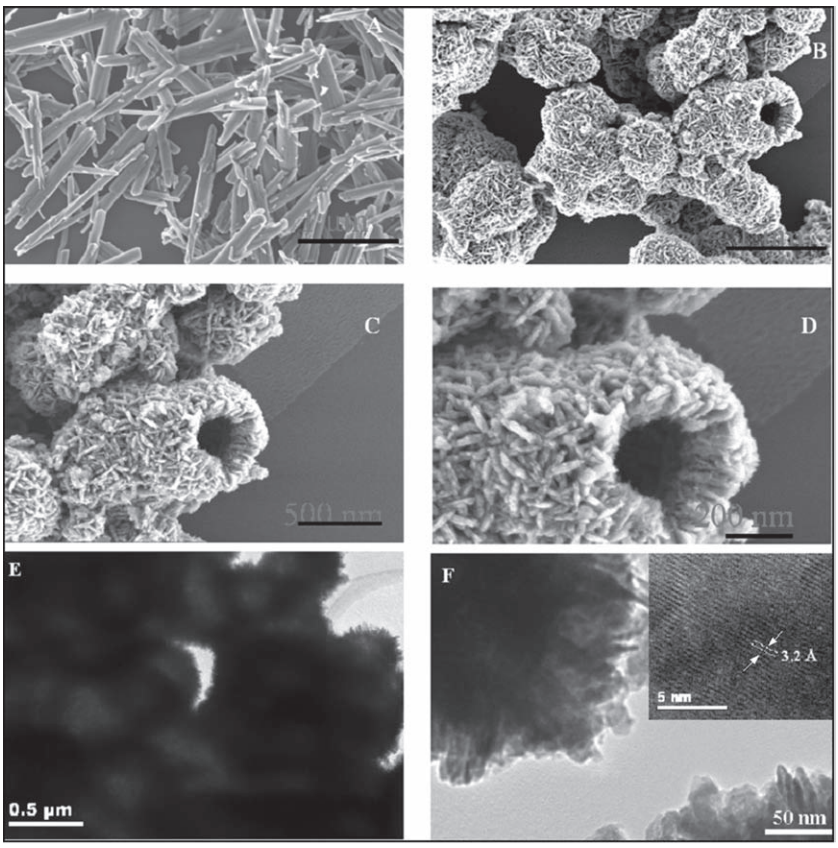

Figure 3. SEM images of γ–MnO_2 spheres. A) morphology of the pure γ-MnO_2; B) overall morphology of TM-1 (8% Ti); C) detailed views on average sized spheres; D) a detailed view on an individual sphere; and E) TEM over all image of the synthesized hollow spheres, F) high magnification of (E).

interpretation of XPS spectra of Ti species present in γ–MnO_2 framework is complex. However, Figure 6b shows the core level spectrum of O 1s, and two binding energies of 530.2 eV and 532.2 eV were observed. The BE of 530.2 eV can be assigned to the Mn-O binding in MnO_2, and the BE of 532.2 eV might belong to the Ti-O-Mn species, suggesting that the Ti species are incorporated into the γ–MnO_2 framework. Because XPS is a surface technique, the photoelectron peaks would depend strongly on the surface concentration of the atoms present, thus making the interpretation of the data with respect to Ti more complicated.

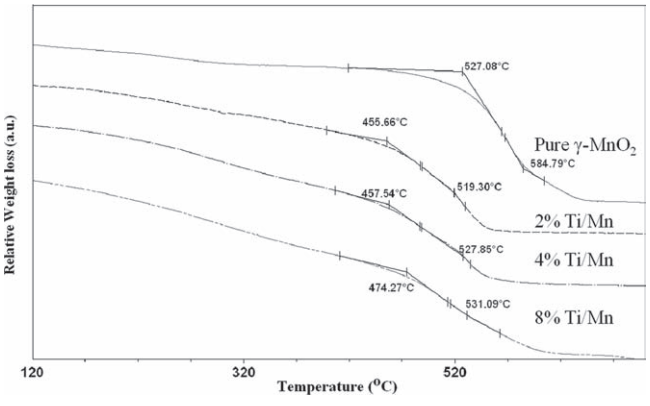

Figure 4. TGA plot of the prepared Ti containing γ–MnO_2 materials.

2.7. Catalytic Results

Electrocatalytic activities of the selected Ti containing γ-MnO_2 (TM-1) were tested in a lithium-air battery. **Table 2** lists the specific capacities in three battery cells. An average specific capacity of 2.2 A h g^{-1} of carbon delivered by using the prepared material as the O_2 reduction catalyst was obtained. The high specific capacity indicates that the material we report here is an efficient O_2 reduction catalyst in the application of Li/air battery. On the other hand, in our previous work, we have reported that γ-MnO_2 was very active in atmospheric toluene oxidation. By using the synthesized γ-MnO_2, 17.6% conversion was achieved. In this work, we compared the Ti incorporated γ-MnO_2 hollow sphere materials with the unincorporated material we reported before. As shown in **Table 3**, the catalytic activity increased from 17% to 31% with increasing Ti content in the materials, indicating that the as-synthesized hollow spheres are more efficient catalysts than a previously reported γ-MnO_2 for toluene oxidation at atmospheric pressure and in an easily operated reaction system.

3. Discussion

3.1. Titanium Incorporation

There are three possible forms for Ti to be present in the products: Free TiO^{2+} cations in the tunnels, framework incorporation in the OMS materials, or TiO_2. The tunnels of γ-MnO_2 with a size of 2.3Å × 2.3Å and 2.3Å × 4.6Å might not accommodate titanium species since the total lengths of Ti-O bonds are around 3.7 Å. On the other hand, γ-MnO_2 does not support ion-exchange activity.[48] After an overnight ion-exchange with 300 mL of 0.5 M sodium sulfate solution, γ-MnO_2 shows similar Ti/Mn molar ratios of about 0.08:1 from EDX results. Therefore, the only possibility for Ti with such a high percentage in the total manganese seems to be incorporation of Ti^{4+} cations into the framework of γ-MnO_2 because the cations in the tunnels can be ion-exchanged with the cations in the solution and Ti/Mn ratio should be decreased after ion-exchange. Similar sizes, charges, and coordination numbers of manganese and Ti cations might contribute to the incorporation of Ti into MnO_6 octahedral units. Crystal radii of octahedral Ti^{4+}, Mn^{3+} and Mn^{4+} in crystals are 0.75 Å, 0.72 Å, and 0.67 Å respectively. Ti^{4+} may substitute for Mn^{4+} without causing much structural disorder or serious charge imbalances as shown in XRD patterns.

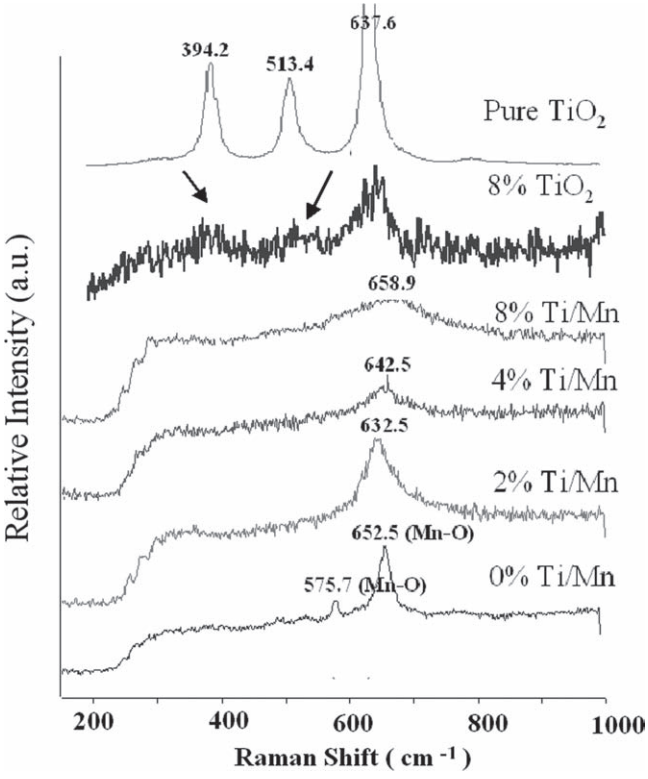

Figure 5. Normalized Raman spectra of the Ti containing γ–MnO_2 hollow spheres.

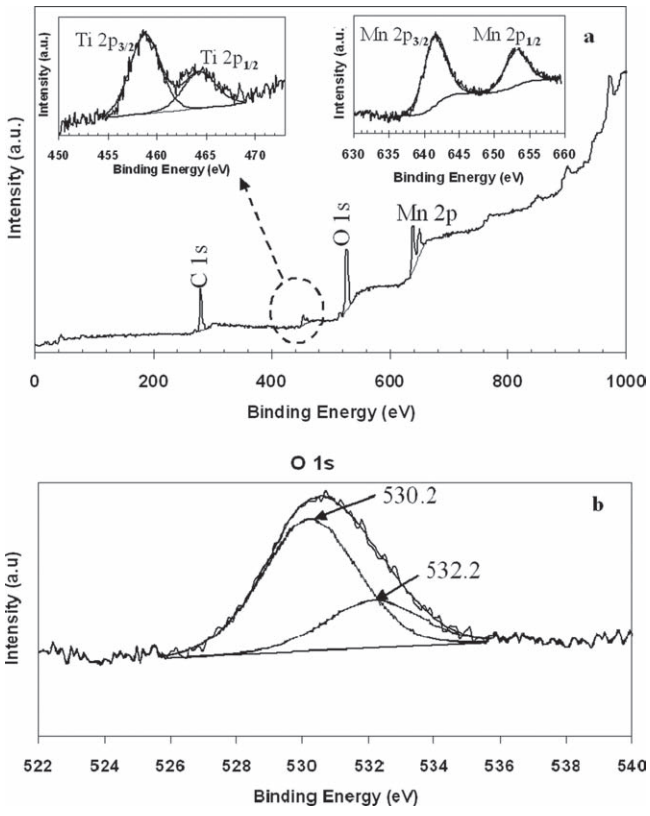

Figure 6. a) XPS survey scan and high-resolution scan (inset) of Ti 2p and Mn 2p; b) XPS high-resolution scan of O 1s. (The C1s peak was used as an internal reference to correct for charge shifts)

TGA measurements of the Ti containing γ-MnO_2 samples showed that with different amounts of Ti content, no extra weight loss peaks were observed. The major weight loss peaks of all the Ti containing γ-MnO_2 materials (TM-1, TM-2, and TM-3) shifted toward lower temperatures than that of the pure γ-MnO_2 material. Among the Ti containing materials, however, the major weight loss peaks slightly increased with a decrease in Ti loading levels. This indicates that the thermal stability of the Ti doped γ-MnO_2 materials is slightly enhanced on increasing the Ti-loading. Physical modifications unlikely cause all these effects. Therefore, there must be some chemical modifications of the γ-MnO_2 structure, such as the introduction of Ti in the crystal structure of γ-MnO_2, in order to make this happen.

Results of Raman spectra also suggested framework titanium incorporation in γ-MnO_2. As shown in Figure 5, no extra stretching vibrational bands which can be indexed to Ti = O bonds (from TiO^{2+} species) or TiO_2 crystal structures were observed. Peaks of MnO_2 located around 600 – 650 cm^{-1} were shifted and broadened with increasing Ti content (larger Ti/Mn molar ratio). The shifted peak position might due to the asymmetric stretching vibration of the Ti-O-Mn bonds. These observations, along with peak broadening, the smaller crystalline size, and the BE of O 1s from XPS results suggest that the titanium might be incorporated into the framework of γ-MnO_2 octahedral molecular sieves.

3.2. Effects of the Reaction Parameters on the Transformation and Structure of the Obtained Titanium Containing γ-MnO_2 Materials

Various amounts of titanium incorporation, distinct metal cation incorporation, various starting Mn^{2+}/Mn^{7+} ratios, and different oxidant precursors have played important roles in determining the morphology and crystal structure of the final

Table 2. Electrocatalytic capacities of the TM-1 material in the Li-air battery test.

Cell ID	Initial Potential [V]	Discharge Capacity [mA h]	Specific Capacity [mA h g^{-1} of Carbon]
1	3.30	57.3	2361
2	3.30	62.5	2317
3	3.30	55.4	1867
			2182

Table 3. Results of toluene atmospheric oxidation by the selected titanium containing γ–MnO_2 (TM-1) materials.

Sample ID	Sel Bzdh [%] [a]	Sel Bzal [%] [b]	Sel Bzad [%] [c]	Conv [%]	TON [d]
undoped – γ-MnO_2	29	20	51	16	19
2% Ti – γ-MnO_2 (TM-3)	23	19	55	17	20
4% Ti – γ-MnO_2 (TM-2)	30	20	49	19	22
8% Ti – γ-MnO_2 (TM-1)	28	17	50	31	36

[a] Benzaldehyde. [b] Benzyl alcohol. [c] Benzoic Acid. [d] Turn over number. *Reaction conditions*: 70 mg of catalysts was mixed ultrasonically in 10 mL toluene and 0.1 mol% AIBN. Reflux at 110 °C for 20 h while bubbling O_2 with constant flow rate of 9 mL min^{-1}. Turn Over Number = mol of converted toluene per mol of catalysts used = (Conv. × 10 mL × 0.87 $g.mL^{-1}$/92.4 g. mol^{-1})/(0.07 g/87 $g.mol^{-1}$).

products. When the amounts of titanium incorporation were varied from 2% to 8% of the total manganese with other parameters unchanged, the structure of the materials did not significantly change based on the XRD pattern shown in Figure 1. The 8% Ti/Mn material has broader XRD peaks than the 2% Ti/Mn material, which can be due to higher surface areas and smaller particle sizes. **Figure 7** shows the SEM images of materials with different ratios of Ti/Mn. Without titanium incorporation, the material is made up of homogenous nanofibers that are around 1 μm in length and 50 nm in diameter. However, with 2% titanium incorporation, the morphology changed to become spherical like materials. With increasing amounts of titanium incorporation, the spherical like materials became more homogeneous, which suggests that the titanium ion is a hollow sphere-like morphology-directing agent for γ-MnO_2.

In order to confirm that titanium ions behave like morphology directing agents, distinct metal ions which have similar ionic radii were also investigated while keeping all the other parameters the same. In the process, we chose V(IV, 0.72 Å), Cr(III, 0.76 Å), Fe(III, 0.79 Å), and Co(III, 0.75 Å) independently whose crystal radii is close to that of Ti(IV, 0.75 Å). **Figure 8** shows the morphology of the materials. As can be seen, none of these materials showed a hollow sphere-like morphology, and only titanium ion acts as a hollow sphere-like morphology directing agent in the synthesis of γ-MnO_2.

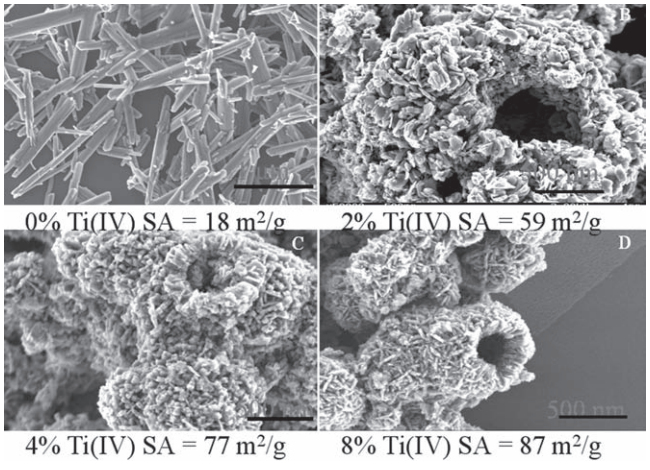

Figure 7. SEM images of γ–MnO_2 spheres with various amounts of titanium.

The titanium containing γ-MnO_2 (TM) was successfully prepared by a simple *in-situ* precipitation method. In acidic media, a redox reaction between MnO_4^- and Mn^{2+} is expected to spontaneously produce MnO_2 based on Equations (3) and (4).

$$MnO_4^-(1) + 4H^+(1) + 3e \rightarrow MnO_2(s) + 2H_2O(1) E^\circ = 1.68V \quad (3)$$

$$MnO_2(s) + 4H^+(1) + 2e \rightarrow Mn^{2+}(1) + 2H_2O(1) E^\circ = 1.22V \quad (4)$$

In this process, $KMnO_4$ solution was designed to be added dropwise into a hot Mn^{2+} solution (85 °C) to provide excess Mn^{2+} during the reaction. A spontaneous redox reaction occurs between the reactants dissolved in water. Since γ-MnO_2 has point defects of Mn^{4+} cations replaced by Mn^{2+} cations,[40] Mn^{4+}/Mn^{2+} replacement occurred immediately with energy provided by heating during the addition of MnO_4^-, γ-MnO_2 was formed.[28]

Herein, we discuss the amount of MnO_4^- addition on γ-MnO_2 structure formation. During the process, we added 150 mL of 0.7 M $KMnO_4$ solution instead of 100 mL into the same amount of Mn^{2+} hot solution with the same feeding rate (0.67 mL min^{-1}) and kept all the other conditions the same. Samples were collected at different times: 1 min, 5 min, 10 min, 15 min, and 20 min. XRD results (**Figure 9**) show that

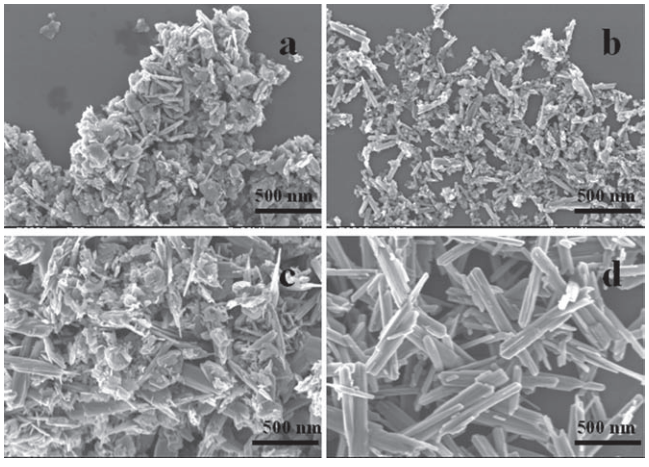

Figure 8. SEM images of γ–MnO_2 with different transit metal ion incorporation. a) 8 at% Fe (III); b) 8 at% V (IV); c) 8 at% Cr (III); d) 8 at% Co (III).

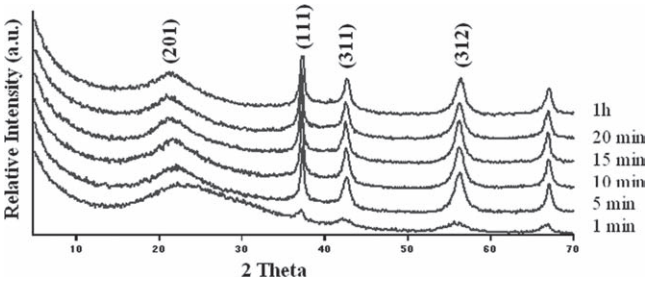

Figure 9. XRD patterns in terms of different reaction time.

the structure did not change in the first 15 min (100 mL $KMnO_4$ solution was added) when using the exact same procedure as before. After 15 min's addition, more $KMnO_4$ was added into the slurry. Since most of the free Mn^{2+} has been precipitated to form γ-MnO_2, Mn^{4+}/Mn^{2+} replacement can not take place because of the lack of excess Mn^{2+}, and the cryptomelane structure started to form, as shown in **Figure 10**.

In an effort to further understand the formation of the γ-MnO_2 crystal structure, we also investigated the effect of oxidants on the γ-MnO_2 structure formation. **Figure 11** shows the XRD results from different oxidants with different reduction potentials. $K_2S_2O_8$ has a higher reduction potential (Equation 5) than that of $KMnO_4$, and the XRD result showed that the γ-MnO_2 structure was maintained, whereas the structure of manganese oxide changed when using the same concentration of $KClO_3$ as the oxidant. Results obtained from using different oxidants indicate that utilization of a strong oxidant is important in formation of the γ-MnO_2 structure.

$$S_2O_8^{2-}(aq) + 2H^+(aq)2e \rightarrow 2HSO_4^-(aq)E \circ \pm = 2.1V \quad (5)$$

$$ClO_3^-(aq) + 3H^+(aq) + 2e \rightarrow HClO_2(aq) + H_2O(1)Eo = 1.24 \quad (6)$$

3.3. Hollow Sphere Structure Evolution

To shed light on the formation mechanism of these novel titanium containing γ-MnO_2 hollow spheres, their growth process

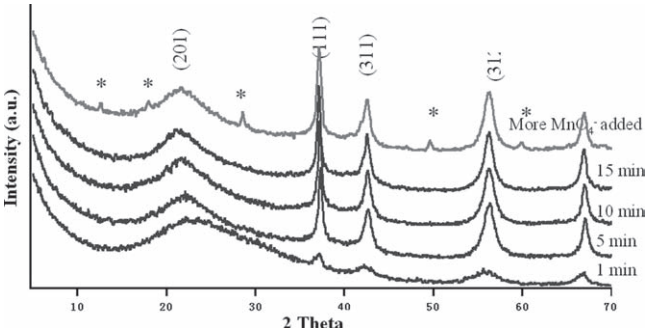

Figure 10. XRD patterns of materials prepared with different oxidants. (*) Cryptomelane MnO_2

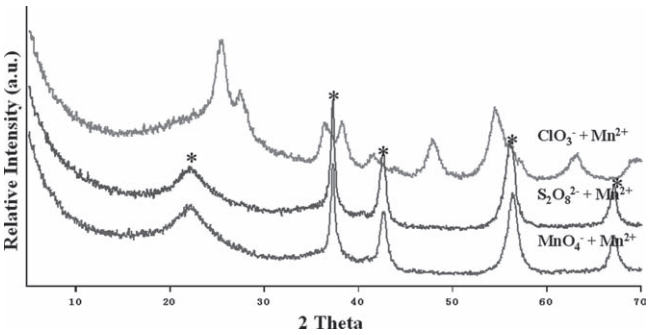

Figure 11. XRD patterns in terms of different amount of oxidants added. (*) γ-MnO_2

has been followed by examining the products harvested at different intervals of reaction times. **Figure 12** shows representative SEM images of the products obtained after various reaction times, which have been demonstrated to be pure γ-MnO_2 crystals by related XRD measurements. From the SEM image of the sample produced at 1 min, we can clearly observe the existence of many small balls, and individual spheres with a diameter of less than 300 nm. After longer refluxing time, the morphologies are more clear, which may be due to increasing crystallinity as shown in XRD (Figure 9).

A self-transformation process by the localized Ostwald ripening could explain the formation mechanism of the titanium containing γ-MnO_2 (TM-1) hollow spheres. Similar mechanisms have been used to prepare different hollow spheres recently.[49–55] The schematic diagram in **Figure 13** shows the possible formation mechanism of the titanium containing γ-MnO_2 (TM-1) hollow sphere. In the beginning (Step 1), MnO_4^- reacts with Mn^{2+} to form nanospheres directed by titanium ions and the nanospheres showed solid interiors as examined by TEM. With addition of more $KMnO_4$ solution, crystallites located on the outermost surface would serve as nucleation seeds for the γ-MnO_2 crystallization process. The outer crystallites started to grow larger after attracting the smaller crystallites underneath, and the continued surface growth on the outer most surface resulted in a core-shell morphology (Step 2). As a result of his process, the core size was then reduced gradually while the vacant volume inside the sphere was enlarged (Step 3), which can be demonstrated by the observation of the morphology through SEM and TEM at a reaction time of 30 min. The vacant space between core and the shell was generated through Ostwald ripening with the mass being transported. The inner core can be easily merged into particles on the outer surface with enough ripening time, and a hollow structure formed (Step 4).

3.4. Electrocatalytic and Oxidative Catalytic Activities

One of the greatest successes for the Ti containing γ-MnO_2 (TM) is the electrocatalytic activity in the Li/air battery test. γ-MnO_2 has been proven to be one of the most useful manganese oxides and has been widely applied in the battery industry due to its high activity.[28] However, among all the manganese oxide based materials, γ-MnO_2 does not have high activity in the

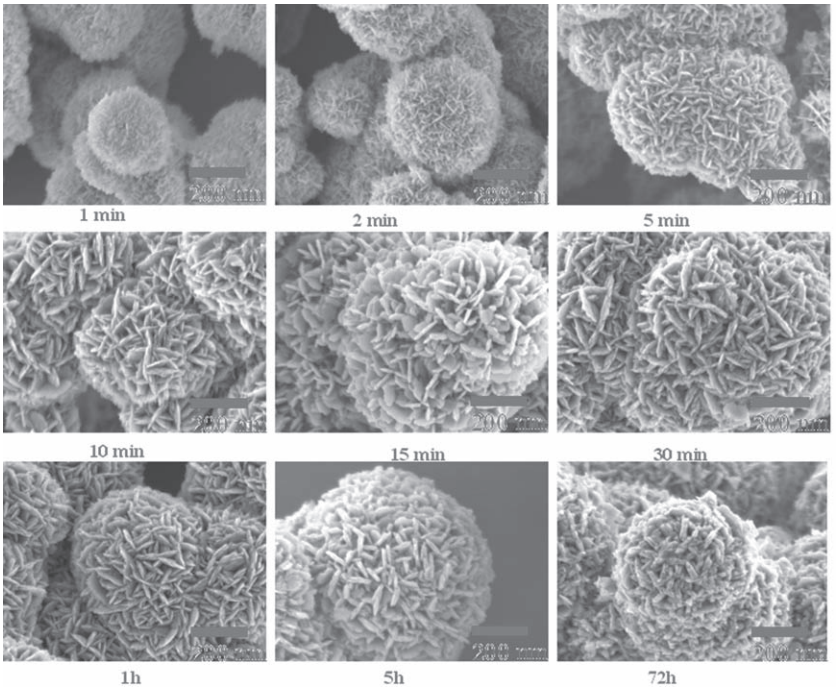

Figure 12. FESEM images for samples prepared at 1 min, 2 min, 5 min, 10 min, 15 min, 30 min, 1h, 5h, and 72h.

electrocatalytic reduction of O_2 in metal-air batteries.[56] Earlier work suggests that γ–MnOOH manganite materials have very high specific capacities (up to 2.2 A h g^{-1} of carbon).[57] Here we tested the selected titanium containing γ-MnO_2 (TM-1) in the same medium-sized lithium-air battery apparatus as reported before. Results are listed in Table 2 and show that capacities up to 2.4 A h g^{-1} of carbon were obtained, indicating similar high electrocatalytic activity of O_2 reduction as that of using γ–MnOOH manganite material earlier reported as catalysts in lithium air battery tests. This is the highest specific capacity reported in Li/air battery tests using γ-MnO_2 based materials as O_2 reduction catalysts.

Another great success for the titanium containing γ-MnO_2 materials is the enhanced oxidative catalytic activities. As reported earlier,[28] solvent free atmospheric toluene oxidation has attracted special attention as a promising environmentally friendly reaction. However, this reaction remains a challenge due to the difficulty of oxidizing sp^3 hybridized carbon in inactive hydrocarbons. Pure γ-MnO_2 prepared by the co-precipitation method was found to be the highest efficient catalyst (17% conversion in 20 h) in earlier work. Here, as can be seen in Table 3, the new Ti containing γ-MnO_2 reported here can catalyze 31% toluene conversion under the same conditions. This much higher oxidative catalytic activity than the pure γ-MnO_2, indicates the strong oxidative activity of this material. In order to further confirm the high oxidative catalytic efficiency of this material, we also studied the selected Ti containing γ-MnO_2 (TM-1, 8 mol% Ti/Mn) as a heterogeneous catalyst for the anisyl alcohol oxidation reaction. A promising high conversion (88%) with high selectivity (100%) on oxidized product (anisic aldehyde) were achieved in 4 h. These are improved catalytic properties as compared to other reported work using manganese oxide based heterogeneous catalysts under the same conditions.[58] Thus, these Ti containing γ-MnO_2 new materials also open up new possibilities for oxidative catalytic reactions.

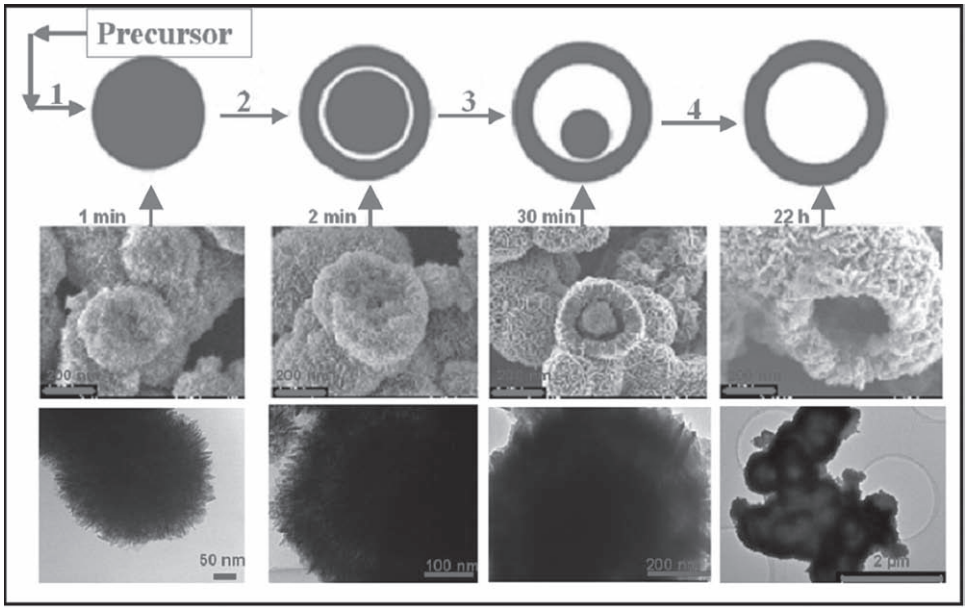

Figure 13. Schematic illustration of the formation process of hollow spheres and the corresponding SEM and TEM images.

4. Conclusions

In conclusion, the Ti-containing γ-MnO_2 (TM) hollow spheres have been successfully synthesized for the first time by a simple co-precipitation method. Titanium cations were used as structure directing agents in the synthesis process. Characterization results suggest that the Ti species were incorporated into the framework of the γ-MnO_2 hollow spheres and no separate anatase or rutile phase were observed. This special structural material prepared by the synthesis procedure disclosed in this paper shows high specific capacity (2.2 A h g^{-1} of carbon) in the Li/air battery tests and strong oxidative catalytic activity in the atmospheric toluene oxidation reaction (conversion of 31% obtained in 20 h reaction, highest conversion reported) in comparison with earlier work. Moreover, a self-transformation process by localized Ostwald ripening can explain the formation mechanism of the titanium containing γ-MnO_2 hollow spheres. This was further characterized by SEM and TEM analyses. This work provides a novel and easy pathway for the synthesis of hollow spheres with strong electrocatalytic and oxidative catalytic activities in Li-air batteries and chemical oxidation reactions respectively, offering a new material platform for batteries and chemical reactions.

5. Experimental Section

Synthesis of the Titanium Containing γ-MnO_2 Octahedral Molecular Sieves: The γ-MnO_2 was prepared by an in situ precipitation method. In a typical synthesis, $MnSO_4$ (3.55 g) was dissolved in 100 mL distilled water, $TiOSO_4.xH_2SO_4$ (Alfa-Aesar, 78 wt.% $TiOSO_4$) was then added into the solution with various Ti/Mn atomic ratios of 2:100 (TM-3), 4:100 (TM-2), and 8:100 (TM-1) at room temperature, along with 6 mL of concentrated nitric acid. The obtained suspension was stirred at room temperature for 1 h until all the $TiOSO_4$ was dissolved and the solution was clear (Solution A). Solution B was prepared by dissolving 1.098 g of potassium permanganate in 100 mL distilled water (0.07 M). The solution B was then added dropwise into the hot aqueous solution A (90 °C, refluxing) in 15 min (flow rate of 6.7 mL min^{-1}) under vigorous stirring. After refluxing the resulting solution for 24 h, the precipitate was filtered and washed with distilled water to remove by-products, followed by drying overnight at 100 °C.

Characterization: The structure of the prepared materials was first analyzed with powder X-ray diffraction (XRD) using a Scintag XDS 2000 diffractometer with a Cu- Kα X-ray source (= 1.5418 nm) and a beam voltage of 45 KV and 40 mA beam current. Morphology of the material was analyzed with a Zeiss DSM 982 Gemini field emission scanning electron microscope (FESEM). Powder specimens were dispersed in ethanol, dropped onto a gold coated silicon wafer, and then the dried wafer was mounted onto a stainless steel sample holder. High resolution transmission electron microscopy (HRSEM) studies were carried out using a JEOL 2010 UHR FasTEM operating at an accelerating voltage of 200 KV and equipped with energy dispersive X-ray spectroscopy (EDS). The samples were prepared by dispersing the material in 2-propanol. Then a drop of the dispersion was placed onto a carbon-coated copper grid and allowed to dry. The chemical composition of the samples was determined by EDS. The surface areas and porsize distributions of the materials were measured using a Micrometritics ASAP 2010 instrument. Samples (100 mg) were pre-degassed at 150 °C for about 10 h to remove water and other physically adsorbed species. The N_2 isothermal adsorption and desorption experiments were performed at relative pressures (P/P_0) from 10^{-3} to 0.995 and from 0.995 to 0.01, respectively. Thermal stability of the synthesized materials was studied with TGA. TGA measurements were conducted in a Hi-Res TGA 2950 thermogravimetric analyzer with 60 mL min^{-1} of N_2 flow from 120 to 700 °C with a heating rate of 10 °C min^{-1}. The Raman spectra were taken at room temperature in the spectral range 100–2000 cm^{-1} using a Renishaw 2000 Raman microscope system, which includes an optical microscope and a CCD camera for multichannel detection. XPS was done on a Leybold-Heraeus model 3000 spectrometer upgraded with a SPECS EA10MCD energy analyzer. The titanium containing γ-MnO_2 powder samples were pressed into indium foil to minimize charging. The average C 1s binding energy found on the indium was used as an internal reference to correct for charge shifts.

The selected Ti containing γ-MnO_2 catalyst (TM-1) was incorporated into hand coated air electrodes for use in Li-air cells following previous procedures.[57] The air cathodes were combined with a Setella separator, and a lithium metal anode, and then placed into a reusable cell case. The electrolyte used was 1 M $LiPF_6$ 1:1:1 EC: DEC: DMC (where EC is ethylene carbonate, DEC is diethyl carbonate, and DMC is dimethyl carbonate). All of the cells built were placed into gas tight bags which were flushed and filled with oxygen gas. In addition all of the cells were placed into a temperature controlled incubator set at 25 °C. The cells were then discharged at a current density of 0.15 mA cm^{-2} using a Maccor test unit.

All the catalytic reactions were carried out in a three-necked round-bottom flask equipped with a condenser; a 9 mL min^{-1} of O_2 flow into the solution at atmospheric pressure, and the flask was placed in an oil bath at a temperature of 110 °C. In a typical reaction, toluene (10 mL, 0.094 mol) with 0.1 mol% of AIBN (2,2'-azobis(isobutyronitrile), a very commonly used radical initiator for the polymerization of vinyl monomers[11]) and 70 mg of catalyst (pretreated at 120 °C for 6 h) were introduced into the reactor. After refluxing for 20 h, the products were dissolved in acetonitrile and analyzed with an HP 5890 Series II gas chromatograph coupled with an HP 5971 mass detector. The column used was a nonpolar cross-linked siloxane (HP-1) with dimensions of 12.5 m × 0.2 m × 0.33 μm.

Acknowledgements

We acknowledge support of the NSF GOALI CBET 0827800, and the Chemical Sciences, Geosciences, and Biosciences Division, Office of Basic Energy Sciences, Office of Science, US Department of Energy. We also thank Yardney Techincal Products, Inc. for lithium air battery tests, Dr. Heng Zhang for the help of XPS analysis, Dr. Francis Galasso, and Dr. Raymond Joesten for many helpful discussions.

Received: May 27, 2010
Revised: June 28, 2010
Published online: August 16, 2010

[1] K. T. Nam, D.-W. Kim, P. J. Yoo, C.-Y. Chiang, N. Meethong, P. T. Hammond, Y.-M. Chiang, A. M. Belcher, *Science* **2006**, *312*, 885.
[2] Y. Xia, B. Gates, Y. Yin, Y. Lu, *Adv. Mater.* **2000**, *12*, 693.
[3] T. Zhang, W. Dong, M. Keeter-Brewer, K. Sanjit, R. N. Njabon, Z. R. Tian, *J. Am. Chem. Soc.* **2006**, *128*, 10960.
[4] H. Shi, L. Qi, J. Ma, H. Cheng, *J. Am. Chem. Soc.* **2003**, *125*, 3450.
[5] D. Qin, H. Tao, Y. Zhao, L. Lan, K. Chan, Y. Cao, *Nanotechnology* **2008**, *19*, 355201.
[6] S. Wang, H. Xu, L. Qian, X. Jia, J. Wang, Y. Liu, W. Tang, *J. Solid State Chem.* **2009**, *182*, 1088.
[7] J. Yuan, K. Laubernds, Q. Zhang, S. L. Suib, *J. Am. Chem. Soc.* **2003**, *125*, 4966.
[8] Y. Zhu, J. Shi, W. Shen, X. Dong, J. Feng, M. Ruan, Y. Li, *Angew. Chem.Int. Ed.* **2005**, *44*, 5083.
[9] H. Li, Z. Bian, J. Zhu, D. Zhang, G. Li, Y. Huo, H. Li, Y. Lu, *J. Am. Chem. Soc.* **2007**, *129*, 8406.
[10] C.-H. Chen, S. F. Abbas, A. Morey, S. Sithambaram, L.-P. Xu, H. F. Garces, W. A. Hines, S. L. Suib, *Adv. Mater.* **2008**, *20*, 1205.
[11] X. Sun, J. Liu, Y. Li, *Chem.–Eur. J.* **2006**, *12*, 2039.

[12] A. D. Dinsmore, M. F. Hsu, M. G. Nikolaides, M. Marquez, A. R. Bausch, D. A. Weitz, *Science* **2002**, *298*, 1006.
[13] D. T. Mitchell, S. B. Lee, L. Trofin, N. Li, T. K. Nevanen, H. Soederlund, C. R. Martin, *J. Am. Chem. Soc.* **2002**, *124*, 11864.
[14] R. A. Caruso, J. H. Schattka, A. Greiner, *Adv. Mater.* **2001**, *13*, 1577.
[15] P. Atienzar, S. Valencia, A. Corma, H. Garcia, *ChemPhysChem* **2007**, *8*, 1115.
[16] T. A. Manz, K. Phomphrai, G. Medvedev, B. B. Krishnamurthy, S. Sharma, J. Haq, K. A. Novstrup, K. T. Thomson, W. N. Delgass, J. M. Caruthers, M. M. Abu-Omar, *J. Am. Chem. Soc.* **2007**, *129*, 3776.
[17] Anon, *Nature* **2008**, *452*, 914.
[18] H. G. Yang, C. H. Sun, S. Z. Qiao, J. Zou, G. Liu, S. C. Smith, H. M. Cheng, G. Q. Lu, *Nature* **2008**, *453*, 638.
[19] J. Y. Kim, K. Lee, N. E. Coates, D. Moses, T.-Q. Nguyen, M. Dante, A. J. Heeger, *Science* **2007**, *317*, 222.
[20] J. Zhuang, G. Yang, D. Ma, X. Lan, X. Liu, X. Han, X. Bao, U. Mueller, *Angew. Chem.Int. Ed.* **2004**, *43*, 6377.
[21] M. G. Clerici, *Stud. Surf. Sci. Catal.* **1993**, *78*, 21.
[22] Y. F. Shen, R. P. Zerger, R. N. DeGuzman, S. L. Suib, L. McCurdy, D. I. Potter, C. L. O'Young, *Science* **1993**, *260*, 511.
[23] O. Giraldo, S. L. Brock, W. S. Willis, M. Marquez, S. L. Suib, S. Ching, *J. Am. Chem. Soc.* **2000**, *122*, 9330.
[24] A. R. Armstrong, P. G. Bruce, *Nature* **1996**, *381*, 499.
[25] R. Ma, Y. Bando, L. Zhang, T. Sasaki, *Adv. Mater.* **2004**, *16*, 918.
[26] Z.-R. Tian, W. Tong, J.-Y. Wang, N.-G. Duan, V. V. Krishnan, S. L. Suib, *Science* **1997**, *276*, 926.
[27] Z.-R. Tian, Y.-G. Yin, S. L. Suib, C. L. O'Young, *Chem. Mater.* **1997**, *9*, 1126.
[28] L. Jin, C.-h. Chen, V. M. B. Crisostomo, L. Xu, Y.-C. Son, S. L. Suib, *Appl. Catal., A* **2009**, *355*, 169.
[29] A. Debart, A. J. Paterson, J. Bao, P. G. Bruce, *Angew. Chem., Int. Ed.* **2008**, *47*, 4521.
[30] T. Ogasawara, A. Debart, M. Holzapfel, P. Novak, P. G. Bruce, *J. Am. Chem. Soc.* **2006**, *128*, 1390.
[31] J. Xiao, D. Wang, W. Xu, D. Wang, R. E. Williford, J. Liu, J.-G. Zhang, *J. Electrochem. Soc. 157*, A487.
[32] J. Read, *J. Electrochem. Soc.* **2006**, *153*, A96.
[33] S. M. George, *Chem. Rev.* **1995**, *95*, 475.
[34] X. Li, J. Xu, F. Wang, J. Gao, L. Zhou, G. Yang, *Catal. Lett.* **2006**, *108*, 137.
[35] G. Huang, A. P. Wang, S. Y. Liu, Y. A. Guo, H. Zhou, S. K. Zhao, *Catal. Lett.* **2007**, *114*, 174.
[36] W. B. Li, W. B. Chu, M. Zhuang, J. Hua, *Catal. Today* **2004**, *93–95*, 205.
[37] X. Li, J. Xu, L. Zhou, F. Wang, J. Gao, C. Chen, J. Ning, H. Ma, *Catal. Lett.* **2006**, *110*, 255.
[38] M. Goethals, B. Vanderstraeten, J. Berghmans, G. De Smedt, S. Vliegen, E. Van't Oost, *J. Hazard. Mater.* **1999**, *70*, 93.
[39] O. Schilling, J. R. Dahn, *J. Appl. Crystallogr.* **1998**, *31*, 396.
[40] P. M. de Wolff, *Acta Crystallogr.* **1959**, *12*, 341.
[41] L. I. Hill, A. Verbaere, *J. Solid State Chem.* **2004**, *177*, 4706.
[42] P. Strobel, J. C. Joubert, M. J. Rodriguez, *J. Mater. Sci.* **1986**, *21*, 583.
[43] A. L. La Salle, S. Sarciaux, A. Verbaere, Y. Piffard, D. Guyomard, *J. Electrochem. Soc.* **2000**, *147*, 945.
[44] M. Polverejan, J. C. Villegas, S. L. Suib, *J. Am. Chem. Soc.* **2004**, *126*, 7774.
[45] H. Yang, D. Tang, X. Lu, Y. Yuan, *J. Phys. Chem. C* **2009**, *113*, 8186.
[46] L. Xia, G. Liu, J. Wang, S. Luo, *J. Raman Spectrosc.* **2009**, *40*, 876.
[47] Y.-Q. Zhang, S.-J. Wang, J.-W. Wang, L.-L. Lou, C. Zhang, S. Liu, *Solid State Sci.* **2009**, *11*, 1412.
[48] W. Buser, P. Graf, *Helv. Chim. Acta* **1955**, *38*, 810.
[49] B. Jia, L. Gao, *J. Phys. Chem. C* **2008**, *112*, 666.
[50] X. Wang, F. Yuan, P. Hu, L. Yu, L. Bai, *J. Phys. Chem. C* **2008**, *112*, 8773.
[51] L. Fan, R. Guo, *J. Phys. Chem. C* **2008**, *112*, 10700.
[52] M. Xu, L. Kong, W. Zhou, H. Li, *J. Phys. Chem. C* **2007**, *111*, 19141.
[53] R. Qiao, X. L. Zhang, R. Qiu, J. C. Kim, Y. S. Kang, *Chem. Mater.* **2007**, *19*, 6485.
[54] C. Lu, L. Qi, J. Yang, X. Wang, D. Zhang, J. Xie, J. Ma, *Adv. Mater.* **2005**, *17*, 2562.
[55] Y. Sui, Y. Zhang, W. Fu, H. Yang, Q. Zhao, P. Sun, D. Ma, M. Yuan, Y. Li, G. Zou, *J. Cryst. Growth* **2009**, *311*, 2285.
[56] L. Mao, T. Sotomura, K. Nakatsu, N. Koshiba, D. Zhang, T. Ohsaka, *J. Electrochem. Soc.* **2002**, *149*, A504.
[57] V. M. B. Crisostomo, J. K. Ngala, S. Alia, A. Dobley, C. Morein, C.-H. Chen, X. Shen, S. L. Suib, *Chem. Mater.* **2007**, *19*, 1832.
[58] E. K. Nyutu, C.-H. Chen, S. Sithambaram, V. M. B. Crisostomo, S. L. Suib, *J. Phys. Chem. C* **2008**, *112*, 6786.